GFD 2006 Lecture 3: Interfacial instability in super-cooled fluid

Grae Worster; notes by Robert Style and Dominic Vella

21 June, 2006

For all the systems that we have considered so far, we have chosen only to model a planar solidification front. In many situations this is not realistic and the interface is in fact subject to instabilities. In this lecture, we consider small perturbations to the planar interface in order to investigate the properties of these instabilities: when do they exist, what is the growth rate of the instability and what is the characteristic length scale? We shall assume non-kinetic growth to simplify the analysis.

1 Mechanism for instability

For a planar solid growing from a cooled boundary, all isotherms in the system are parallel to the solid–liquid interface (see Fig. 1). When we introduce a perturbation onto the interface, the isotherms are deformed in response to the new boundary conditions (as shown in Fig. 1b). As a result of this, the isotherms are bunched where the solid protrudes into the liquid (crests) and are spread out where the solid lags behind (troughs). In the regions where the isotherms are bunched, the temperature gradient is large and so there will be enhanced heat transport from liquid to solid relative to the heat transport in the planar system. The protrusion is therefore eroded. Similarly, less heat will be transported to the troughs and so the rate of solidification is locally increased. These effects act to stabilize the interface by levelling out any deviation from the steady planar state.

For the case of a supercooled melt, the heat flows from the solid towards the liquid. As before, upon introduction of the perturbation, there is bunching of the isotherms above crests on the solid–liquid interface and enhanced spacing of isotherms above the troughs. However, the directions of the heat fluxes are reversed from the previous case, so that heat is transported more rapidly away from the crests and more slowly away from the troughs. This causes the interface to advance more rapidly at the crests, and relatively slower at the troughs, so that any corrugations will grow in amplitude (Fig. 1c). Thus the interface is unstable.

In the student exercise from the previous lecture, we saw that perturbations are stabilized due to the Gibbs-Thomson effect. We found that the curvature of the interface modifies the equilibrium melting temperature to

$$T_e = T_m - \Gamma \nabla \cdot \mathbf{n}, \tag{1}$$

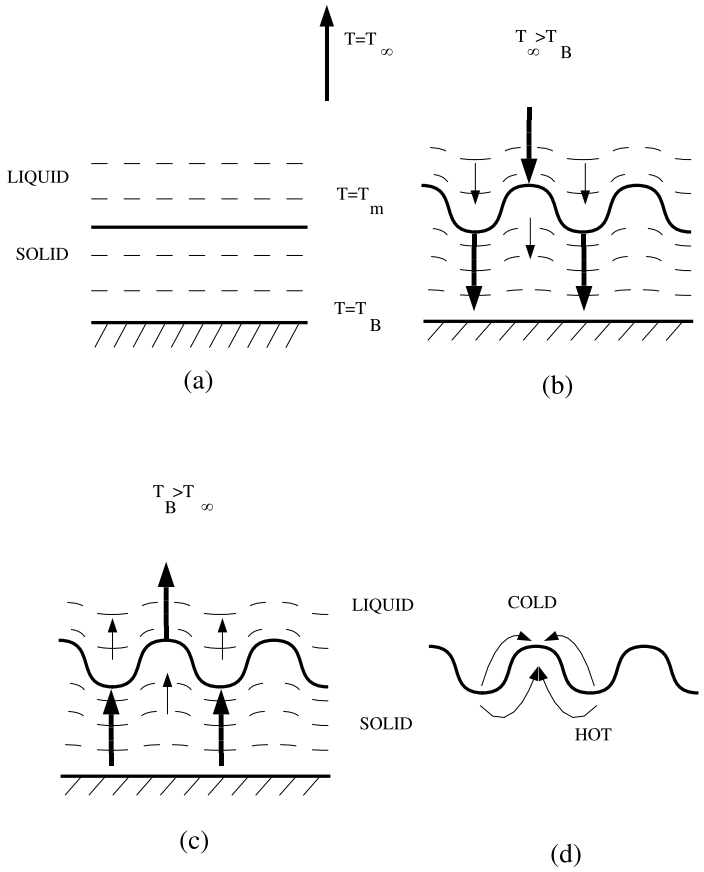

Figure 1: Schematic diagrams showing the direction of heat flow (arrows) during the evolution of the solid–liquid interface. (a) Planar solidification from a cooled front. (b) Stability of a front growing from a cooled boundary. (c) Instability of a front growing into a supercooled melt. (d) Stabilization as a result of the Gibbs-Thomson effect.

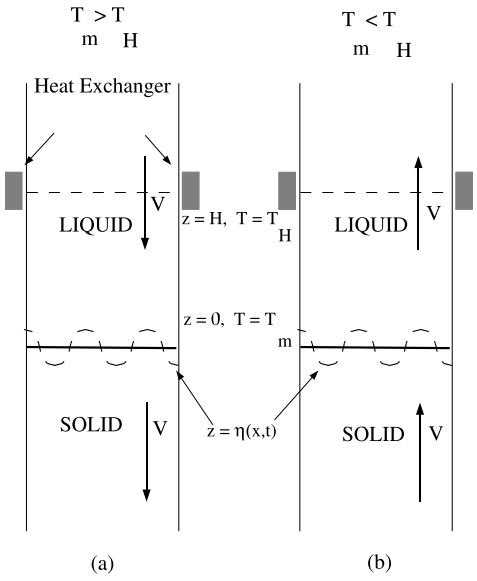

Figure 2: Schematic diagram for (a) solidification of liquid by pulling liquid downwards through a cooled heat exchanger and (b) melting of solid by pulling upwards through a heated heat exchanger.

where $\nabla \cdot \mathbf{n}$ is the interface curvature. Therefore, the interface temperature is reduced relative to T_m at crests in the interface and increased at troughs. Thus heat will flow from troughs to crests, causing the crests to melt back, while the troughs solidify faster, stabilizing the front (see Fig. 1d). In the following, we will consider the stability of a planar front growing into a supercooled melt including the Gibbs-Thomson effect. As will be seen, the Gibbs-Thomson effect stabilizes the front for small wavelengths, while the front becomes unstable at longer wavelengths.

2 Modelling interfacial instability

In order to explore stability of a planar surface growing into a supercooled melt, we consider the case of liquid being pulled down through a heat exchanger at a constant velocity V as shown in Fig. 2. The heat exchanger maintains the temperature at $T_H < T_m$ at a height $z = H$, and the interface is assumed to be initially planar at $z = 0$. In experiments it is V, rather than the position of the interface, H, which is controlled and so H is an unknown: in this problem, it will be determined from the Stefan boundary condition.

If we apply a small perturbation $z = \eta(x, t)$ to the solid–liquid interface, we can investigate the stability of the interface as follows. The pulling velocity introduces an advective term into the heat equation, which becomes:

$$\frac{\partial T}{\partial t} - V\frac{\partial T}{\partial z} = \kappa \nabla^2 T, \tag{2}$$

while the boundary conditions are

$$T = T_H \quad \text{at} \quad (z = H), \tag{3}$$

$$T = T_m - \Gamma \nabla \cdot \mathbf{n} \quad \text{at} \quad (z = \eta), \tag{4}$$

and

$$\rho L(V + \eta_t) = -k \left. \frac{\partial T}{\partial z} \right|_{z=\eta}. \tag{5}$$

Note that we have already linearized the Stefan boundary condition for small perturbations by assuming that the normal to the interface is parallel to the z-axis.

In order to non-dimensionalize the equations, we choose to scale lengths with H, time with SH^2/κ and write $T = T_H + (T_m - T_H)\theta$. In terms of these nondimensional variables, the advection–diffusion equation then becomes

$$\frac{1}{S}\frac{\partial \theta}{\partial t} - p\frac{\partial \theta}{\partial z} = \nabla^2 \theta, \tag{6}$$

while the Stefan boundary condition takes the form

$$Sp + \eta_t = -\theta_z, \tag{7}$$

where the Peclet number is defined as $p = VH/\kappa$ and measures the strength of advection relative to diffusion. The remaining boundary conditions can then be written as

$$\theta = 1 - \gamma \boldsymbol{\nabla} \cdot \boldsymbol{n} \quad (z = \eta), \tag{8}$$

$$\theta = 0 \quad (z = 1), \tag{9}$$

where $\gamma = \Gamma/H\Delta T$ is the non-dimensional surface energy.

We initially seek a steady state such that $\theta = \theta(z)$ has no t or x dependence and $\eta = 0$. Equation (6) then simplies to

$$\theta'' + p\theta' = 0 \tag{10}$$

and the temperature field in the liquid is given by

$$\theta = 1 - \frac{1 - e^{-pz}}{1 - e^{-p}}. \tag{11}$$

We can then apply the Stefan boundary condition to obtain the Peclet number (and thus the interface velocity) in terms of the Stefan number as

$$p = -\log(1 - S^{-1}). \tag{12}$$

When the Stefan number is large, we can expand Eqn. (12) in terms of S^{-1} to show that $p \approx S^{-1} \ll 1$. Therefore, when we consider Eqn. (6) in the large S limit, we can discard the time derivative and advection terms (the quasi-stationary approximation) to approximate the temperature field as

$$\theta \approx 1 - z. \tag{13}$$

With this quasi–stationary approximation, we can now perform a linear stability analysis by applying a small disturbance

$$\eta = \hat{\eta} e^{i\alpha x + \sigma t} \tag{14}$$

to the interface and letting the temperature field take the form

$$\theta = 1 - z + \hat{\theta} e^{i\alpha x + \sigma t}. \tag{15}$$

Substituting this expression for θ into the quasi–stationary form of Eqn. (6), we obtain

$$\hat{\theta}'' - \alpha^2 \hat{\theta} = 0, \tag{16}$$

so that

$$\hat{\theta} = A \sinh \alpha (1 - z), \tag{17}$$

in which we have applied the boundary condition at $z = 1$.

In order to determine the curvature of the interface, we note that for an interface determined by the equation $g(x, z, t) = 0$, the normal to the surface is given by

$$\boldsymbol{n} = \frac{\boldsymbol{\nabla} g}{|\boldsymbol{\nabla} g|}.$$

Here, $g = z - \eta(x, t)$ and so

$$\mathbf{n} = \frac{(-\eta_x, 1)}{(1 + \eta_x^2)^{1/2}} \approx (-\eta_x, 1), \tag{18}$$

while the curvature, $\mathcal{K} = \boldsymbol{\nabla} \cdot \boldsymbol{n}$ takes the form

$$\boldsymbol{\nabla} \cdot \boldsymbol{n} \approx -\eta_{xx}. \tag{19}$$

Using this expression for the curvature, we can apply the two remaining boundary conditions at the solid–liquid interface in order to obtain a dispersion relation controlling the rate of growth of the individual wavelengths. The Stefan condition gives

$$\sigma \hat{\eta} = -\hat{\theta}' = \alpha A \cosh \alpha, \tag{20}$$

and the Gibbs–Thomson condition gives that

$$\hat{\theta} - \hat{\eta} = -\gamma(-\eta_{xx}) = -\alpha^2 \gamma \hat{\eta},$$

which becomes

$$A \sinh \alpha - \hat{\eta} = -\alpha^2 \gamma \hat{\eta}. \tag{21}$$

Combining Eqns. (20) and $\sigma \times$(21), we obtain

$$A\sigma \sinh \alpha - \alpha A \cosh \alpha = -\alpha^3 \gamma A \cosh \alpha, \tag{22}$$

from which we immediately have the dispersion relation

$$\sigma = \alpha \coth \alpha (1 - \gamma \alpha^2). \tag{23}$$

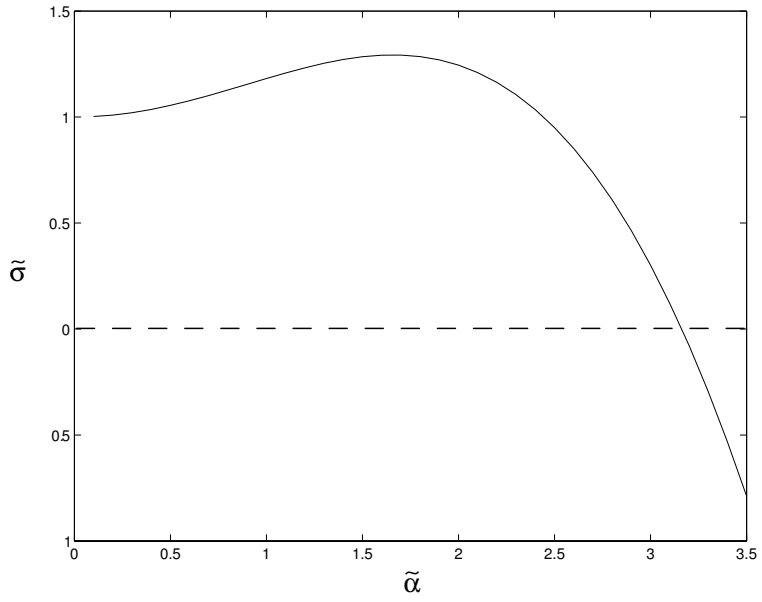

Figure 3: Plot of the dispersion relation (23) in the case $\gamma = 0.1$.

This can be simplified in the limits of small and large wavelength perturbations to

$$\sigma = \begin{cases} -\gamma\alpha^3, & \alpha \gg 1 \\ 1 + \alpha^2\left(\frac{1}{3} - \gamma\right), & \alpha \ll 1. \end{cases} \tag{24}$$

Equation (23) can be used to plot the dependence of σ on α, as demonstrated in Fig. 3. In particular, we note two interesting properties of equation (23). Firstly, there is a critical wavenumber, α_c, above which $\sigma < 0$ and perturbations decay in time; the interface is stable for $\alpha > \alpha_c$. There is therefore a minimum wavelength below which the instability is eliminated. Clearly,

$$\alpha_c = \gamma^{-1/2}. \tag{25}$$

We can then write the minimum wavelength, λ_c, in dimensional terms as

$$\lambda_c = \frac{2\pi H}{\alpha_c} = 2\pi\left(H\ell_c\right)^{1/2}, \tag{26}$$

where

$$\ell_c \equiv \frac{\gamma_{sl}}{\rho L}\frac{T_m}{\Delta T} = \gamma H \tag{27}$$

is the capillary length. The minimum wavelength is therefore proportional to the geometric mean of the capillary length and H, which is a lengthscale for thermal diffusion. Typically for ice we have

$$\ell_c = \frac{(3\times10^{-2}\text{ N m}^{-1})\times(300\text{ K})}{(10^3\text{ kg m}^{-3})\times(3\times10^5\text{ J kg}^{-1})\times(1\text{ K})} \sim 30\text{ nm}. \tag{28}$$

In typical laboratory experiments, $H \sim 10^{-1}$ m and so we find that the minimum wavelength $\lambda_c \sim 300$ μm.

Secondly, we observe from Fig. 3 that there is a maximally unstable wavenumber, α_m, provided that $\gamma < 1/3$. Expanding (23) for $\alpha_m \gg 1$ and requiring that $\sigma'(\alpha_m) = 0$, we find that

$$\alpha_m = (3\gamma)^{-1/2} = \frac{\alpha_c}{\sqrt{3}}. \tag{29}$$

This wavenumber corresponds to a maximally unstable wavelength $\lambda_m = \sqrt{3}\lambda_c$. Since it is this mode that grows fastest, this is the wavelength that we might expect to observe in experiments. Recall also that typically $\ell_c \sim 30$ nm and $H \sim 0.1$ m so that

$$\gamma = \frac{\ell_c}{H} \sim 10^{-7} \ll 1, \tag{30}$$

and our approximation that $\alpha_m \gg 1$ is valid. Finally, we find that $\lambda_m \approx 0.5$ mm for typical laboratory experiments.

Student Problem *Show that a melting interface is stable by considering the above problem with $T_H > T_m$ and V with the opposite sign. (cf. Fig. 2b.)*

Solution We note that the system is effectively identical to the previous case, except that now $\tilde{V} = -V$ and $\tilde{\Delta T} = (T_H - T_m) = -\Delta T$, where tilde/no tilde distinguishes between the melting/freezing problem, respectively. We also see that $\tilde{p} = -p$, $\tilde{S} = -S$ and we can define $T = T_H - \tilde{\Delta T}\tilde{\theta}$. Thus when we non-dimensionalize the equations (and dropping tildes), we find that

$$\frac{1}{S}\frac{\partial \theta}{\partial t} + p\frac{\partial \theta}{\partial z} = \nabla^2\theta, \tag{31}$$

$$Sp - \eta_t = -\theta_z \quad (z = \eta), \tag{32}$$

$$\theta = 1 + \gamma \boldsymbol{\nabla} \cdot \boldsymbol{n} \quad (z = \eta), \tag{33}$$

and

$$\theta = 0 \quad (z = 1). \tag{34}$$

There is a steady state solution as before, such that

$$\theta = 1 - \left(\frac{1 - e^{pz}}{1 - e^{p}}\right), \tag{35}$$

and upon applying the Stefan boundary condition, we find that

$$p = \log(1 + S^{-1}) \tag{36}$$

so that $p \approx S^{-1}$ for $S \gg 1$.

As before, for large S, we can make a quasi-staionary approximation by discarding time derivative and advection terms in the diffusion–advection equation so that:

$$\theta \approx 1 - z. \tag{37}$$

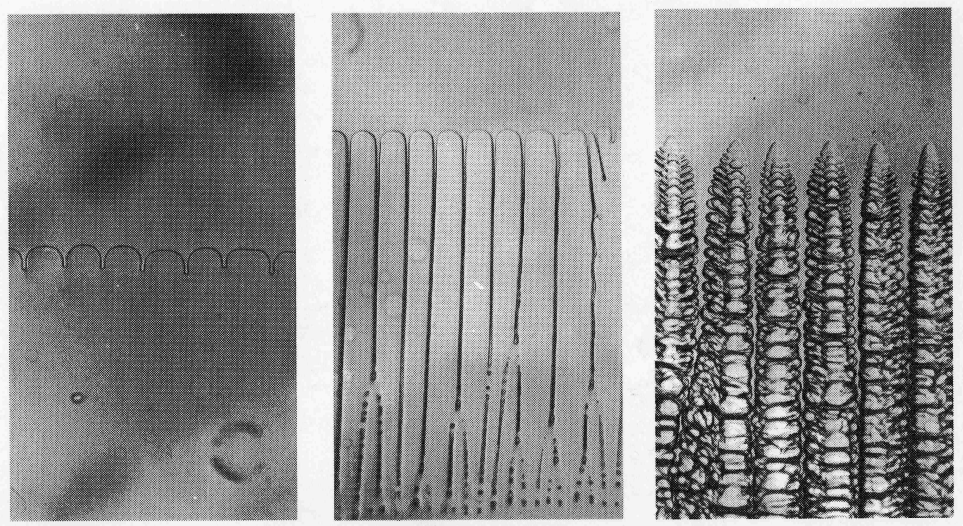

Figure 4: Photographs showing the development of the morphological instability discussed here. In the middle picture, pinching is observed leaving inclusions of liquid within the solid.

Finally, using this linear approximation as a basic state, we apply a small perturbation to the interface of the form

$$\eta = \hat{\eta} e^{i\alpha x + \sigma t} \tag{38}$$

along with

$$\theta = 1 - z + \hat{\theta} e^{i\alpha x + \sigma t} \tag{39}$$

which yields a similar dispersion relation to the freezing case:

$$\sigma = -\alpha \coth \alpha (1 + \gamma \alpha^2). \tag{40}$$

Note that the expression for σ is always negative, and so the interface is stable to small amplitude perturbations of all wavelengths.

3 Beyond linear theory: pinching

The morphological instability discussed in the last section is manifested as a fingering instability with typical finger morphologies shown in Fig. 4. As these fingers grow, their growth cannot any longer be understood by the linear stability analysis presented in the last section. Instead, nonlinearities become important and the fingers themselves become unstable to dendritic growth shown in Fig. 4. While the detailed morphology of these fingers is difficult to understand without detailed numerical simulations, the pinching instability of the fingers (illustrated in the middle frame of Fig. 4) can be understood by means of a simple model. This pinching is of particular interest since it results in pockets of fluid being trapped within the solid. Here we present a simple model of pinching, which is mathematically analogous to the model of the pinching of a liquid thread developed by Rayleigh and Plateau.

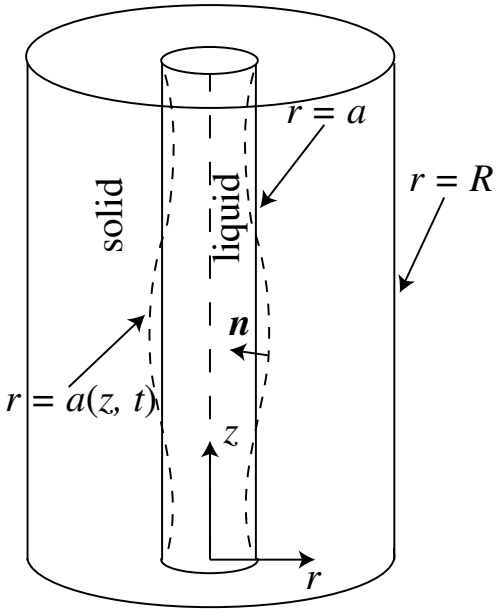

Figure 5: Setup showing the one dimensional model of pinching in solidification.

We consider a liquid cylinder of radius a within a concentric annulus of inner and outer radii a and $R > a$ respectively, as shown in Fig. 5. This is the simplest geometry that will lead to an instability since in two dimensions the surface energy acts to suppress pinching. With a third dimension, however, there are two competing curvatures: an axisymmetric perturbation in the cylinder radius increases the 'ring' curvature where the radius is smallest driving fluid away from that point and driving the instability further. We assume that the material properties of the two phases are identical.

The interface between liquid and solid is given by

$$g(r, z, t) = a(z, t) - r = 0, \tag{41}$$

where we are assuming that the system remains axisymmetric for all times. The normal (pointing from solid to liquid) is then given by

$$\boldsymbol{n} = \frac{(-1, a_z)}{\sqrt{1 + a_z^2}}, \tag{42}$$

so that

$$\begin{aligned} \boldsymbol{\nabla} \cdot \boldsymbol{n} &= \frac{1}{r}\frac{d}{dr}\left(r\frac{-1}{\sqrt{1+a_z^2}}\right) + \frac{d}{dz}\left(\frac{a_z}{\sqrt{1+a_z^2}}\right) \\ &\approx -\frac{1}{r} + a_{zz} \approx -\frac{1}{a} + a_{zz}. \end{aligned}$$

The (equilibrium) temperature along the interface is therefore given by

$$T_e \approx T_m + \Gamma\left(\frac{1}{a} - a_{zz}\right). \tag{43}$$

This expression has to be combined with the conservation of heat to obtain a complete set of equations. For long wavelength deformations, the system has time to equilibriate across cross-sections at fixed z and so we assume that $T = T(z)$. The conservation of heat is considerably simplified by this approximation. In particular, if $H_{l,s}$ represents the specific enthalpy in the liquid/solid phases, then the conservation of heat for an element of height δz requires that

$$\rho\frac{\partial}{\partial t}\left[\pi a^2\delta z H_l + \pi(R^2-a^2)\delta z H_s\right] = \left[q(z) - q(z+\delta z)\right]\pi R^2, \tag{44}$$

where $q = -k\partial T/\partial z$ is the conductive heat flux in the system. Taking the limit $\delta z \to 0$, we find that

$$\rho(H_l - H_s)\frac{\partial}{\partial t}\left(\pi a^2\right) + \pi a^2\rho\frac{\partial H_l}{\partial t} + \pi(R^2-a^2)\rho\frac{\partial H_s}{\partial t} = -\pi R^2\frac{\partial q}{\partial z}. \tag{45}$$

However, by definition we have $H_l - H_s = L$ and $(\partial H/\partial T)_p = c_p$ so that (45) first simplifies to

$$\rho L\frac{\partial}{\partial t}(\pi a^2) + \pi R^2\rho c_p\frac{\partial T}{\partial t} = \pi R^2\frac{\partial}{\partial z}\left(k\frac{\partial T}{\partial z}\right),$$

and then

$$\rho c_p\frac{\partial T}{\partial t} = \frac{\partial}{\partial z}\left(k\frac{\partial T}{\partial z}\right) - \rho L\frac{\partial}{\partial t}\left(\frac{\pi a^2}{\pi R^2}\right). \tag{46}$$

This can in turn be written in terms of the solid volume fraction $\phi = 1 - a^2/R^2$ to give

$$\rho c_p\frac{\partial T}{\partial t} = \frac{\partial}{\partial z}\left(k\frac{\partial T}{\partial z}\right) + \rho L\frac{\partial \phi}{\partial t}. \tag{47}$$

Note that (47) has the diffusive character of the heat equation that we have solved previously. However, we now have a source of heat arising from the latent heat produced in the conversion of liquid into solid. In this respect, (47) is very similar to the conservation of heat in a mushy layer, which we shall meet in a few lectures' time.

Under the assumption that there are no kinetic effects, T and a are related through the Gibbs-Thomson equation (43). We can therefore eliminate T from (46) in favour of a and rewrite (46) as a single equation for $a(z,t)$:

$$\rho c_p\Gamma\frac{\partial}{\partial t}\left(\frac{1}{a} - a_{zz}\right) = k\Gamma\frac{\partial^2}{\partial z^2}\left(\frac{1}{a} - a_{zz}\right) - \frac{\rho L}{R^2}\frac{\partial}{\partial t}(a^2). \tag{48}$$

If we perturb the initially cylindrical fluid inclusion then we can write $a(z,t) = a_0 + a_1(z,t)$ (where a_0 is a constant). Substituting this expression into (48) and linearizing, we find that

$$\rho c_p\Gamma\frac{\partial}{\partial t}\left(\frac{a_1}{a_0^2} - a_{1,zz}\right) = k\Gamma\frac{\partial^2}{\partial z^2}\left(\frac{a_1}{a_0^2} - a_{1,zz}\right) + \frac{2\rho L}{R^2}a_0 a_{1,t}. \tag{49}$$

We can then look for normal mode solutions with $a_1 \propto \exp(\mathrm{i}\alpha x + \sigma t)$. The resulting dispersion relation is simplified by non-dimensionalizing lengths with R and times with

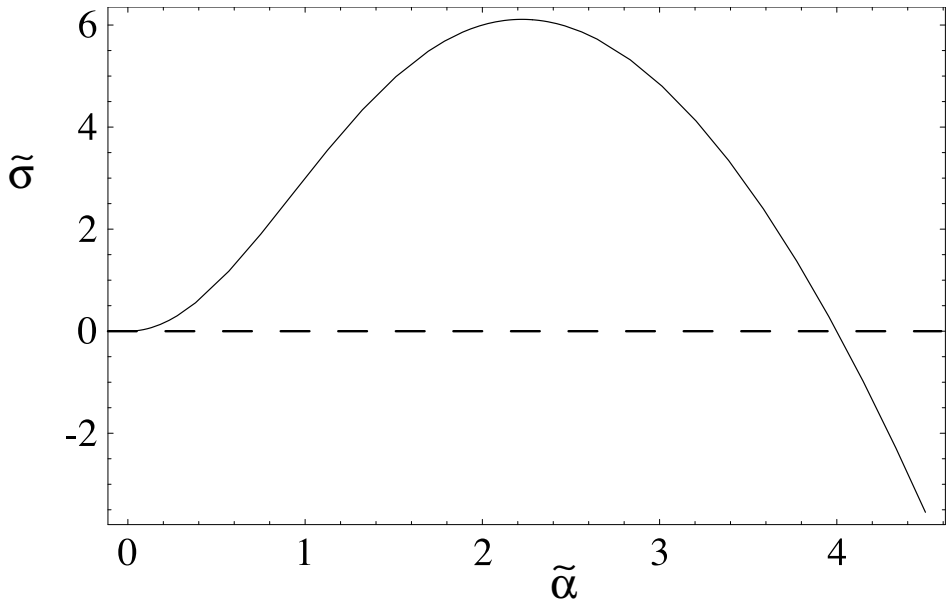

Figure 6: The dispersion relation (50) showing the existence of a maximally unstable wavenumber. Here $\tilde{a}_0 = 0.25$ and $\mathcal{S} = 10$, so that (52) is satisfied.

R^2/κ — the thermal diffusion timescale. Denoting dimensionless quantities with $\tilde{}$ we find that

$$\tilde{\sigma} = \tilde{\alpha}^2 \frac{1 - \tilde{a}_0^2 \tilde{\alpha}^2}{(2\mathcal{S} + \tilde{\alpha}^2)\tilde{a}_0^2 - 1}, \tag{50}$$

where

$$\mathcal{S} \equiv \frac{LR}{c_p \Gamma} \tag{51}$$

is the relevant Stefan number in this problem. This dispersion relation is plotted in figure 6. Again, considering the behaviour of $\tilde{\sigma}(\tilde{\alpha})$ in the limits $\tilde{\alpha} \ll 1$ and $\tilde{\alpha} \gg 1$ reveals that there is a maximally unstable wavenumber in this problem, provided that

$$\mathcal{S} > \tfrac{1}{2} a_0^{-2}. \tag{52}$$

We expect that this maximally unstable wavenumber would give rise to a well-defined wavelength in experiments.